Polarimetric dimension and nonregularity of tightly focused light beams

Yahong Chen* and Fei Wang
School of Physical Science and Technology and Collaborative Innovation Center of Suzhou Nano Science and Technology, Soochow University, Suzhou 215006, China

Zhen Dong and Yangjian Cai†
School of Physical Science and Technology and Collaborative Innovation Center of Suzhou Nano Science and Technology, Soochow University, Suzhou 215006, China
and Shandong Provincial Engineering and Technical Center of Light Manipulation and Shandong Provincial Key Laboratory of Optics and Photonic Device, School of Physics and Electronics, Shandong Normal University, Jinan 250014, China

Andreas Norrman
Photonics Laboratory, ETH Zurich, CH-8093 Zurich, Switzerland

José J. Gil
Department of Applied Physics, University of Zaragoza, Pedro Cerbuna 12, 50009 Zaragoza, Spain

Ari T. Friberg and Tero Setälä‡
Institute of Photonics, University of Eastern Finland, P.O. Box 111, FI-80101 Joensuu, Finland

(Received 21 February 2020; accepted 1 April 2020; published 11 May 2020)

Polarimetric dimension and nonregularity are newly introduced concepts that characterize three-dimensional (3D) polarization states of light. We analyze the spectral polarimetric dimension and the degree of nonregularity associated with two kinds of tightly focused beams: a radially fully polarized Gaussian Schell-model (GSM) beam and a partially polarized beam composed of an incoherent superposition of two orthogonally polarized (coherent) plane-wave modes. We show that for both beams the focal field can exhibit genuine 3D and nonregular character, with even perfect nonregularity encountered for the tightly focused two-mode beam. These features originate from the partial spatial coherence and partial polarization of the incident beams, and in the limit of full coherence and polarization the three-dimensionality and nonregularity of the focal field vanish. We also find that the GSM beam can generate a nanoscale region around the focus where the field is essentially 3D unpolarized. The results demonstrate the rich polarimetric structure of focal fields and may find uses in optical particle manipulation and sensing.

DOI: 10.1103/PhysRevA.101.053825

I. INTRODUCTION

Three-dimensional (3D) random light is specified by the physical property that the electric field fluctuates in three orthogonal spatial directions at a single point in any reference frame. While the polarization theory of optical beams (planar light fields) is well developed [1,2], the polarimetric description of 3D fields has attracted considerable interest only recently due to the increasing importance of nonparaxial light fields and near-field situations [3]. Among the novel findings on 3D light is that the indices of purity provide quantitative information on the polarimetric purity, while qualitative insight is gained via the components of purity [2,4,5]. The field's apparent dimensionality (intensity-distribution spread in 3D space) can be characterized with the polarimetric dimension [6,7] and a new view on the 3D polarimetric structure is achieved via the notion of nonregularity and the associated degree of nonregularity [4,8,9]. Quite recently it was demonstrated that a random evanescent wave created in total internal reflection of a partially polarized planar field is always in a 3D [6] and nonregular [10] polarization state.

In this work, we consider another frequently encountered situation in which genuine 3D fields with a high degree of nonregularity may be expected, namely, tightly focused random light beams. Such fields have found a diversity of important applications. For example, a radially polarized beam can generate a strong longitudinal focal component and a small transverse spot size [11,12]. Focal fields may exhibit polarization Möbius strips [13], novel spin and orbital angular momentum effects [14,15], and they have been employed for instance in optical particle manipulation [16] and nanoscopic sensing [17]. Specifically, we evaluate the spectral polarimetric dimension and nonregularity of two different types of

*yahongchen@suda.edu.cn
†yangjiancai@suda.edu.cn
‡tero.setala@uef.fi

tightly focused fields. In the first case we take the incident beam to be a radially fully polarized Gaussian Schell-model (GSM) beam, and in the second scenario we consider a partially polarized beam composed of two orthogonal, mutually uncorrelated plane-wave modes. The focusing is treated within the Richards-Wolf formalism [3,18–20], combined with a recently introduced fast calculation algorithm [21]. For both beam types, genuine 3D and nonregular focal fields are found. A GSM beam can generate an almost 3D-unpolarized field around the focal point, while for a partially polarized two-mode beam even perfect nonregularity can be achieved at some locations. The true 3D and nonregular features vanish when the incident beam becomes completely polarized and spatially coherent, which is expected as the ensuing fully polarized focal electric field is necessarily restricted to a plane at every point [6].

The work is organized as follows. In Sec. II, we recall the polarimetric dimension and the notion of nonregularity. In Sec. III, the model beams are presented and the Richards-Wolf formalism for tight focusing is outlined. Section IV discusses the behavior of the polarimetric quantities in the focal plane for the two incident model beams. Finally, Sec. V summarizes the main findings.

II. POLARIMETRIC QUANTITIES

The spectral polarization properties of a random three-component electromagnetic field, at a point $\mathbf{r}$, are described by the 3×3 polarization matrix

$$\mathbf{\Phi}(\mathbf{r}, \omega) = \langle \mathbf{E}^*(\mathbf{r}, \omega)\mathbf{E}^{\mathrm{T}}(\mathbf{r}, \omega)\rangle, \tag{1}$$

where $\mathbf{E}(\mathbf{r}, \omega) = [E_x(\mathbf{r}, \omega), E_y(\mathbf{r}, \omega), E_z(\mathbf{r}, \omega)]^{\mathrm{T}}$ represents the electric field at angular frequency ω. The angle brackets, asterisk, and superscript T stand for the ensemble average, complex conjugate, and transpose, respectively. The polarization matrix is a Hermitian matrix whose eigenvalues are nonnegative and we take them to be ordered as $\lambda_1 \geqslant \lambda_2 \geqslant \lambda_3$. The related (orthonormal, column) eigenvectors are denoted by $\hat{\mathbf{u}}_1$, $\hat{\mathbf{u}}_2$, and $\hat{\mathbf{u}}_3$. From now on we do not, for brevity, explicitly show the frequency dependence of spectral quantities.

A. Polarimetric dimension

The polarimetric dimension, quantifying the apparent dimensionality or the intensity spread of a light field, can be expressed as [6]

$$D = 3 - \frac{\sqrt{2[(a_1 - a_2)^2 + (a_1 - a_3)^2 + (a_2 - a_3)^2]}}{a_1 + a_2 + a_3}, \tag{2}$$

where $a_1 \geqslant a_2 \geqslant a_3$ are the eigenvalues of $\mathrm{Re}[\mathbf{\Phi}(\mathbf{r})]$ with Re denoting the real part. For simplicity the spatial dependence of various quantities is omitted here. This notation will be adopted in many places also later. The eigenvalues are the intensities of the Cartesian field components in the frame where the coordinate axes coincide with the principal axes of the ellipsoid representing the intensity distribution of the field. The polarimetric dimension is bounded as $1 \leqslant D \leqslant 3$, with the lowest value $D = 1$ corresponding to one-dimensional (1D) light, i.e., linearly polarized light ($a_2 = a_3 = 0$), while the largest value $D = 3$ is associated with 3D intensity-isotropic light ($a_1 = a_2 = a_3$) [7]. For two-dimensional (2D) light the electric field vector is in a plane ($a_3 = 0, a_2 > 0$) and the polarimetric dimension satisfies $1 < D \leqslant 2$, with the case $D = 2$ signifying a 2D intensity-isotropic field ($a_2 = a_3$), such as a circularly polarized or an unpolarized beam. Values obeying $2 < D \leqslant 3$ are thus manifestations of genuine 3D light fields ($a_3 > 0$) whose three components have nonzero intensity for any orientation of the Cartesian reference frame. We remark, however, that 3D light can also assume $1 < D \leqslant 2$ if the intensity distribution is anisotropic. The polarimetric dimension is invariant under coordinate rotations since they do not change the polarization state, whereas the polarization-changing unitary operations may change the D value.

B. Polarimetric nonregularity

Insight into the structure of the 3×3 polarization matrix is provided by the characteristic decomposition [5]

$$\mathbf{\Phi}(\mathbf{r}) = I[P_1\hat{\mathbf{\Phi}}_p + (P_2 - P_1)\hat{\mathbf{\Phi}}_m + (1 - P_2)\hat{\mathbf{\Phi}}_u], \tag{3}$$

where $I = \lambda_1 + \lambda_2 + \lambda_3$ is the intensity and

$$P_1 = (\lambda_1 - \lambda_2)/I, \quad P_2 = 1 - 3\lambda_3/I \tag{4}$$

are the indices of polarimetric purity satisfying $0 \leqslant P_1 \leqslant P_2 \leqslant 1$ [22]. Furthermore,

$$\hat{\mathbf{\Phi}}_p = \hat{\mathbf{u}}_1\hat{\mathbf{u}}_1^\dagger, \tag{5}$$

$$\hat{\mathbf{\Phi}}_m = \tfrac{1}{2}(\hat{\mathbf{u}}_1\hat{\mathbf{u}}_1^\dagger + \hat{\mathbf{u}}_2\hat{\mathbf{u}}_2^\dagger), \tag{6}$$

$$\hat{\mathbf{\Phi}}_u = \tfrac{1}{3}(\hat{\mathbf{u}}_1\hat{\mathbf{u}}_1^\dagger + \hat{\mathbf{u}}_2\hat{\mathbf{u}}_2^\dagger + \hat{\mathbf{u}}_3\hat{\mathbf{u}}_3^\dagger) = \tfrac{1}{3}\mathbf{I}, \tag{7}$$

where the dagger stands for conjugate transpose and $\mathbf{I}$ is the 3×3 identity matrix. The matrices $\hat{\mathbf{\Phi}}_p$ and $\hat{\mathbf{\Phi}}_u$ describe, respectively, a fully polarized (pure) state and a completely unpolarized 3D state. The interpretation of $\hat{\mathbf{\Phi}}_m$, called the discriminating component, requires more attention and leads to the classification of the 3D polarization states into regular and nonregular states, as introduced in the time domain in [4,8]. These state types were thoroughly discussed in [9] and analyzed in the context of evanescent waves in [10]. Excluding the special (regular-field) case $P_1 = P_2$, a field is regular if $\hat{\mathbf{\Phi}}_m$ is an equiprobable mixture of two orthogonal states whose polarization ellipses lie in the same plane. In this case $\hat{\mathbf{\Phi}}_m$ is real valued and represents a 2D unpolarized state. For a nonregular field $\hat{\mathbf{\Phi}}_m$ is complex valued and corresponds to an incoherent mixture of two equal-intensity states whose polarization ellipses are confined to different planes. Hence, for a nonregular state $\hat{\mathbf{\Phi}}_m$ does not describe 2D unpolarized light but true 3D light. The discriminating state $\hat{\mathbf{\Phi}}_m$ is said to be perfectly nonregular when it is an equiprobable mixture of a circularly polarized state and a mutually orthogonal linearly polarized state.

The degree of nonregularity of the discriminating component $\hat{\mathbf{\Phi}}_m$ is defined as $P_N(\hat{\mathbf{\Phi}}_m) = 4\hat{m}_3$, where $0 \leqslant \hat{m}_3 \leqslant 1/4$ is the smallest eigenvalue of $\mathrm{Re}(\hat{\mathbf{\Phi}}_m)$, while the degree of nonregularity of the full state $\mathbf{\Phi}(\mathbf{r})$ is given by [9]

$$P_N = (P_2 - P_1)P_N(\hat{\mathbf{\Phi}}_m). \tag{8}$$

Both degrees are bounded between 0 and 1, with the lower limit corresponding to a regular state. The extreme case $P_N = 1$ is found exclusively for a state $\mathbf{\Phi}(\mathbf{r}) = I\hat{\mathbf{\Phi}}_m$ with $P_N(\hat{\mathbf{\Phi}}_m) =$

1, in which case not only the discriminating state $\hat{\mathbf{\Phi}}_m$ but also the whole state $\mathbf{\Phi}(\mathbf{r})$ itself is a perfect nonregular state.

The degree of nonregularity and polarimetric dimension of $\hat{\mathbf{\Phi}}_m$ are related as [9]

$$D(\hat{\mathbf{\Phi}}_m) = 3 - \sqrt{1 - \tfrac{3}{4}P_N(\hat{\mathbf{\Phi}}_m)[2 - P_N(\hat{\mathbf{\Phi}}_m)]}. \tag{9}$$

Consequently, if $\hat{\mathbf{\Phi}}_m$ describes a nonregular polarization state, i.e., $P_N(\hat{\mathbf{\Phi}}_m) > 0$, then necessarily $2 < D(\hat{\mathbf{\Phi}}_m) \leqslant 5/2$, indicating that $\hat{\mathbf{\Phi}}_m$ represents a field with genuine 3D character. Furthermore, since Eq. (9) implies that $P_N(\hat{\mathbf{\Phi}}_m)$ can be expressed solely in terms of $D(\hat{\mathbf{\Phi}}_m)$, we find that also the degree of nonregularity of the total state P_N in Eq. (8) is directly connected to the polarimetric dimension of the discriminating component.

III. BEAM MODELS AND FOCUSING

We consider the polarimetric dimension and the degree of nonregularity in the focal region for two types of incident beams. One is a radially fully polarized but spatially partially coherent GSM beam, whereas the other is a partially polarized beam composed of two orthogonally linearly polarized, mutually uncorrelated plane-wave fields. In this section, we describe the associated 2×2 cross-spectral density matrices (CSDMs), defined as [23,24]

$$\mathbf{W}(\mathbf{r}_1, \mathbf{r}_2) = \langle \mathbf{E}^*(\mathbf{r}_1)\mathbf{E}^{\mathrm{T}}(\mathbf{r}_2)\rangle, \tag{10}$$

where $\mathbf{E}(\mathbf{r}) = [E_x(\mathbf{r}), E_y(\mathbf{r})]^{\mathrm{T}}$ represents the (transverse) electric vector of a beam taken to propagate along the z axis.

The CSDM of a partially coherent beam can be decomposed into a sum of CSDMs corresponding to spatially fully coherent field modes which are mutually uncorrelated. The advantage of this representation is that the various propagation and focusing problems involving partially coherent beams can then be analyzed in terms of coherent optics by considering the individual modal vector functions. In such a mode representation, the coherence matrix in Eq. (10) can be expressed in the series form as

$$\mathbf{W}(\mathbf{r}_1, \mathbf{r}_2) = \sum_n \alpha_n \boldsymbol{\mathcal{E}}_n^*(\mathbf{r}_1)\boldsymbol{\mathcal{E}}_n^{\mathrm{T}}(\mathbf{r}_2), \tag{11}$$

where $\boldsymbol{\mathcal{E}}_n(\mathbf{r})$ and α_n are the mode vectors and their weights, respectively. The above expression is called the pseudo-mode representation if the mode vectors are not orthonormal in the region of interest. These representations have attracted significant attention recently [25], and they have been adopted in many circumstances involving partially coherent fields [26–30]. The traditional coherent-mode representation [23,24] likewise has the form of Eq. (11), but the modes are orthonormal and satisfy a Fredholm integral equation. Below we also briefly summarize the focusing procedure of the mode vectors. A detailed description can be found in [21].

A. Radially fully polarized GSM beam

We take the CSDM of a radially polarized GSM beam to be of the form [31,32]

$$\mathbf{W}(\mathbf{r}_1, \mathbf{r}_2) = \sqrt{\mathcal{S}(\mathbf{r}_1)\mathcal{S}(\mathbf{r}_2)}\, g(\Delta\mathbf{r})\hat{\mathbf{e}}_r(\mathbf{r}_1)\hat{\mathbf{e}}_r^{\mathrm{T}}(\mathbf{r}_2), \tag{12}$$

where

$$\mathcal{S}(\mathbf{r}) = \left(2r^2/w_0^2\right)\exp\left(-2r^2/w_0^2\right) \tag{13}$$

denotes the (doughnut-shaped) spectral density with w_0 characterizing the beam width and $r = |\mathbf{r}|$. In addition,

$$\hat{\mathbf{e}}_r(\mathbf{r}) = \cos\phi\hat{\mathbf{e}}_x + \sin\phi\hat{\mathbf{e}}_y \tag{14}$$

is the unit (radial) polarization vector of the beam at point $\mathbf{r}$, with ϕ being the azimuthal angle with respect to the x axis, and $\hat{\mathbf{e}}_x$ and $\hat{\mathbf{e}}_y$ are the x and y Cartesian unit vectors. The function $g(\Delta\mathbf{r})$, with $\Delta\mathbf{r} = \mathbf{r}_1 - \mathbf{r}_2$, represents the complex degree of coherence of the beam and its absolute value equals the frequency-domain version of the electromagnetic degree of coherence defined in [33]. For a GSM beam, we have

$$g(\Delta\mathbf{r}) = \exp\left[-(\Delta\mathbf{r})^2/\left(2\delta_0^2\right)\right], \tag{15}$$

where δ_0 stands for the transverse coherence width of the beam.

We construct the vectorial modes for the radially polarized GSM beam by adopting the recently advanced complex random screens decomposition [34,35]. The technique allows one to write the degree of coherence $g(\Delta\mathbf{r})$ as an incoherent sum of factored-form functions representing statistically independent stochastic screens. This procedure, described in [21], enables one to express the CSDM in Eq. (12) in the form of Eq. (11), where the modal weights satisfy $\alpha_n = 1$, for all n, and the mode vectors are

$$\boldsymbol{\mathcal{E}}_n(\mathbf{r}) = \sqrt{\mathcal{S}(\mathbf{r})/N}\,\mathcal{T}_n(\mathbf{r})\hat{\mathbf{e}}_r(\mathbf{r}). \tag{16}$$

Above, N is the total number of screens and $\mathcal{T}_n(\mathbf{r})$ is the scalar transmittance function of the screen of index n. The transmittances are obtained via $\mathcal{T}_n(\mathbf{r}) = \int \tau_n(\mathbf{f})\exp(i2\pi\mathbf{r}\cdot\mathbf{f})d^2\mathbf{f}$, with $\tau_n(\mathbf{f}) = [a_n(\mathbf{f}) + ib_n(\mathbf{f})]\sqrt{p(\mathbf{f})/2}$ being a complex random function of spatial frequency $\mathbf{f}$. Here $a_n(\mathbf{f})$ and $b_n(\mathbf{f})$, with $n = 1, \ldots, N$, constitute two sets of real Gaussian random variables each having unit variance and zero mean. The sets are independent in the sense that the variables in one are independent of those in the other. The combination of $a_n(\mathbf{f})$ and $b_n(\mathbf{f})$ with fixed n defines a complex circular Gaussian random variable. In addition, $p(\mathbf{f})$ is the (deterministic) power spectrum associated with the complex random screens, given by $p(\mathbf{f}) = \int g(\Delta\mathbf{r})\exp(-i2\pi\,\Delta\mathbf{r}\cdot\mathbf{f})d^2\Delta\mathbf{r}$.

B. Incoherent superposition of orthogonally polarized plane-wave modes

We assume a field composed of well-collimated x and y orthogonally polarized, mutually uncorrelated plane waves. The electric-field components for this field can be written as

$$\mathbf{E}_j(\mathbf{r}) = E_j\exp(ik_0z)\hat{\mathbf{e}}_j, \quad j \in \{x, y\}, \tag{17}$$

where the amplitude E_j is a random variable and $k_0 = \omega/c$ is the wave number with c denoting the vacuum speed of light. Since E_x and E_y are uncorrelated, the CSDM at a plane transverse to the propagation direction assumes the form

$$\mathbf{W}(\mathbf{r}_1, \mathbf{r}_2) = \begin{pmatrix} W_{xx} & 0 \\ 0 & W_{yy} \end{pmatrix}, \tag{18}$$

where $W_{jj} = \langle E_j^* E_j\rangle$, with $j \in \{x, y\}$. Because both field components are fully coherent, they can be expressed in the

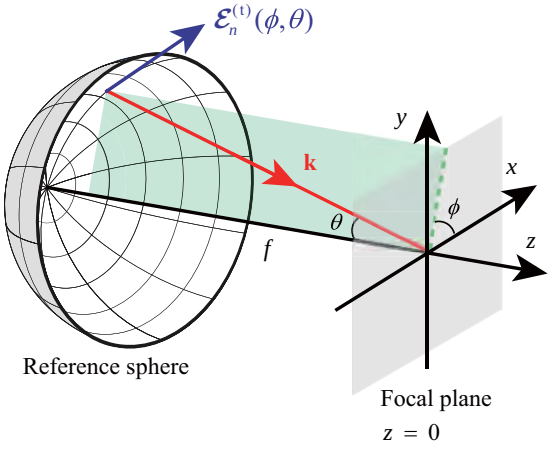

FIG. 1. Geometry related to focusing a mode vector $\boldsymbol{\mathcal{E}}_n(\mathbf{r})$ by an aplanatic lens of focal length f. The focal plane is at $z = 0$. The mode vector transmitted through the lens is $\boldsymbol{\mathcal{E}}_n^{(t)}(\phi,\theta)$. The (wave) vector $\mathbf{k}$ specifies the direction of a plane wave (ray) emanating from a point on the reference sphere and is expressed in terms of the angles ϕ and θ.

factored form $W_{jj} = \mathcal{E}_j^* \mathcal{E}_j$, where $\mathcal{E}_j$ is a complex number. In view of the representation in Eq. (11), the beam contains two modes given by the constant vectors

$$\boldsymbol{\mathcal{E}}_1(\mathbf{r}) = \mathcal{E}_x \hat{\mathbf{e}}_x, \quad \boldsymbol{\mathcal{E}}_2(\mathbf{r}) = \mathcal{E}_y \hat{\mathbf{e}}_y, \tag{19}$$

and the weights $\alpha_1 = \alpha_2 = 1$. In the simulations we set $\mathcal{E}_y = 1$ and vary $\mathcal{E}_x$ whose phase is set to zero.

Since the CSDM is constant, it equals the polarization matrix as $\boldsymbol{\Phi}(\mathbf{r}) = \mathbf{W}(\mathbf{r}, \mathbf{r})$. The degree of polarization of the incident beam therefore can be written as [23]

$$P_{2D} = \frac{|W_{xx} - W_{yy}|}{W_{xx} + W_{yy}}. \tag{20}$$

The degree is bounded between 0 and 1 with the extreme values referring to a fully 2D unpolarized and fully polarized beam, respectively.

C. Richards-Wolf formalism for tight focusing

Next we briefly recall the Richards-Wolf formalism for computing the strongly focused field distribution produced by an aplanatic objective lens (or an optical system). More detailed descriptions can be found in the literature [3,18,19]. The transmission through the lens is treated within the ray picture and the lens is taken to obey the sine condition, i.e., the incident rays are refracted at the reference sphere whose radius equals the focal length f of the lens, as illustrated in Fig. 1. We assume that the medium preceding the lens is vacuum while the refractive index after it is n_t. An incident spatially fully coherent mode $\boldsymbol{\mathcal{E}}_n(\mathbf{r})$ propagating along the z axis is decomposed into the radially and azimuthally polarized constituents, with the related polarization unit vectors $\hat{\mathbf{e}}_r$ [Eq. (14)] and $\hat{\mathbf{e}}_\phi = -\sin\phi \hat{\mathbf{e}}_x + \cos\phi \hat{\mathbf{e}}_y$, respectively. In transmission the radial polarization unit vector tilts at the off-axial points and acquires a longitudinal (z) component, whereas the azimuthal polarization unit vector remains in the original direction. These vectors, corresponding to a plane wave (ray) propagating away from the reference sphere at a point determined by (ϕ, θ), can be written as $\hat{\mathbf{e}}_r^{(t)} = \cos\theta \hat{\mathbf{e}}_r + \sin\theta \hat{\mathbf{e}}_z$ and $\hat{\mathbf{e}}_\phi^{(t)} = \hat{\mathbf{e}}_\phi$. The angle θ is bounded between 0 and $\theta_{\max} = \arcsin(\mathrm{NA}/n_t)$, with NA being the numerical aperture of the lens. Thus, the mode after the reference sphere becomes $\boldsymbol{\mathcal{E}}_n^{(t)}(\phi,\theta) = t_r \mathcal{E}_n^{(\mathrm{rad})}(\phi,\theta)\hat{\mathbf{e}}_r^{(t)} + t_\phi \mathcal{E}_n^{(\mathrm{azi})}(\phi,\theta)\hat{\mathbf{e}}_\phi^{(t)}$, where $\mathcal{E}_n^{(\mathrm{rad})}(\phi,\theta)$ and $\mathcal{E}_n^{(\mathrm{azi})}(\phi,\theta)$ are the amplitudes of the radial and azimuthal components of the incident mode, respectively, while t_r and t_ϕ are the transmission coefficients for the two polarization directions. Due to the power conservation requirement and the sine condition, $t_r = t_\phi = \sqrt{\cos\theta/n_t}$ holds.

The mode vector in the focal region is obtained by inserting $\boldsymbol{\mathcal{E}}_n^{(t)}(\phi,\theta)$ into the Richards-Wolf diffraction integral [36]

$$\boldsymbol{\Psi}_n(\boldsymbol{\rho}, z) = -\frac{if}{2\pi n_t} \iint_{|\mathbf{k}_\perp| \leqslant \Omega} \boldsymbol{\mathcal{E}}_n^{(t)}(k_x, k_y) \exp(ik_z z) k_z^{-1} \times \exp[-i(k_x x + k_y y)] dk_x dk_y, \tag{21}$$

where $\boldsymbol{\rho} = (x, y)$, $\mathbf{k}_\perp = (k_x, k_y)$, and $\Omega = 2\pi\mathrm{NA}/\lambda$ with $\lambda = 2\pi c/\omega$. The location on the reference sphere is represented in terms of the wave-vector components $k_x = -k\sin\theta\cos\phi$, $k_y = -k\sin\theta\sin\phi$, and $k_z = k\cos\theta$ with $k = 2\pi n_t/\lambda$. The transformation from the angles to the wave-vector space was made in order to conform to the fast calculation algorithm put forward in [21]. The integration in Eq. (21) is limited to the directions covered by the numerical aperture.

The CSDM near the focal region can be evaluated as

$$\mathbf{W}^{(f)}(\boldsymbol{\rho}_1, z_1; \boldsymbol{\rho}_2, z_2) = \sum_n \alpha_n \boldsymbol{\Psi}_n^*(\boldsymbol{\rho}_1, z_1) \boldsymbol{\Psi}_n^{\mathrm{T}}(\boldsymbol{\rho}_2, z_2). \tag{22}$$

The polarization matrix in the focal region is readily obtained through $\boldsymbol{\Phi}(\boldsymbol{\rho}, z) = \mathbf{W}^{(f)}(\boldsymbol{\rho}, z; \boldsymbol{\rho}, z)$.

IV. SIMULATION RESULTS

In this section, we present the simulation results concerning the polarimetric dimension and nonregularity in the focal plane of the tightly focused beams described in Sec. III. The parameters of the focusing geometry in Fig. 1 are taken to be $\mathrm{NA} = 0.95$, $f = 3$ mm, and $n_t = 1$, whereas the wavelength of both beams is $\lambda = 632.8$ nm. For the radially fully polarized GSM beam, the beam width is fixed at $w_0 = 1$ mm.

A. Radially fully polarized GSM beam

Figures 2(a)–2(f) show the spatial distributions of the polarimetric dimension D of Eq. (2) in the focal plane $z = 0$ for a tightly focused radially polarized GSM beam whose transverse coherence length δ_0 is 10, 2, 1.3, 1.0, 0.5, and 0.05 mm, respectively. The high-intensity region where the intensity is larger than 10% of its maximum value is depicted with a dashed circle. In Figs. 3(a)–3(f) the gray dashed, blue dotted, and purple dash-dotted curves show the coefficients P_1, $P_2 - P_1$, and $1 - P_2$ of the characteristic decomposition in Eq. (3) along the positive x axis in the focal plane for the above coherence lengths. These facilitate explaining the content of Fig. 2.

In general, the contours of the polarimetric dimension in Fig. 2 display rings in all cases. When the radially polarized incident beam is spatially highly coherent, the focus field is

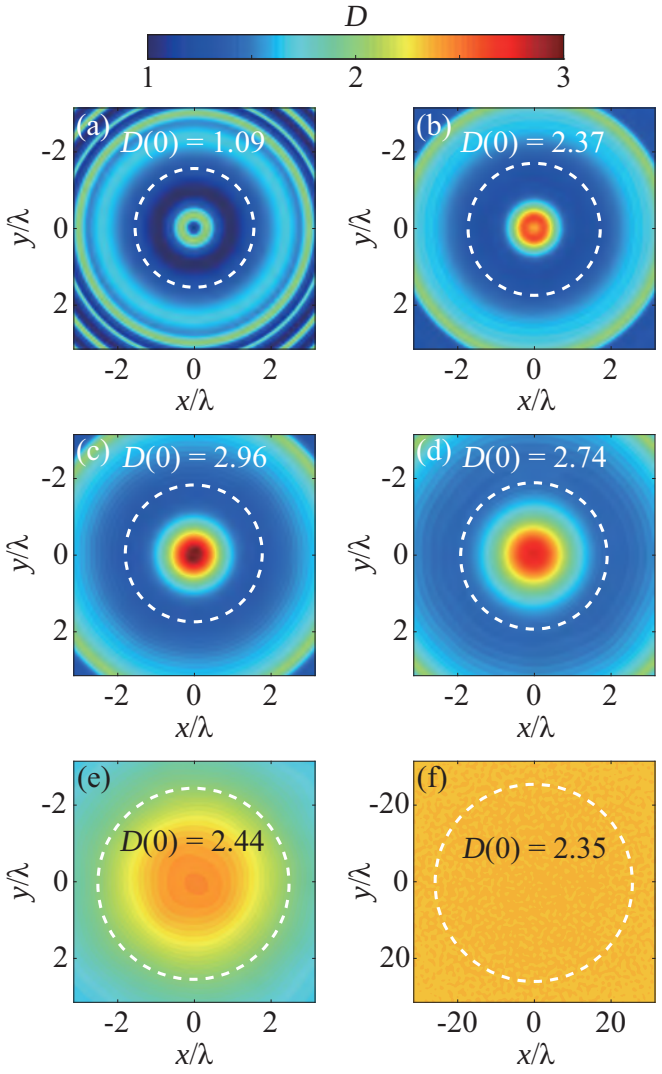

FIG. 2. Spatial distribution of the polarimetric dimension D in the focal plane ($z = 0$) of a tightly focused radially polarized GSM beam, with the spatial coherence width δ_0 of (a) 10 mm, (b) 2 mm, (c) 1.3 mm, (d) 1.0 mm, (e) 0.5 mm, and (f) 0.05 mm. Inside the dashed circle the intensity is larger than 10% of its maximum value and $D(0)$ indicates the polarimetric dimension in the focal point. Notice the different length scale in (f).

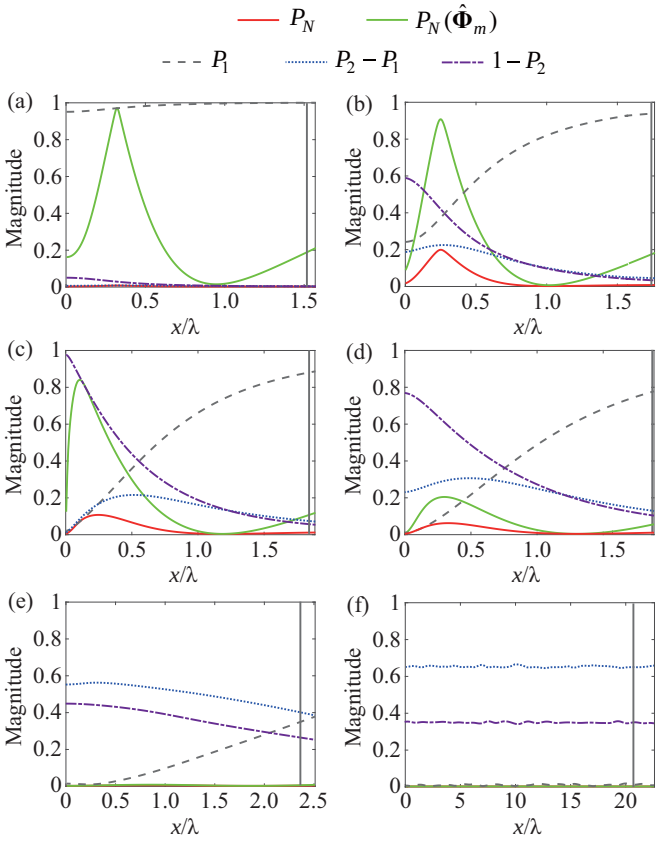

FIG. 3. Behavior of the degrees of nonregularity P_N and $P_N(\hat{\mathbf{\Phi}}_m)$, and the coefficients P_1, $(P_2 - P_1)$, and $(1 - P_2)$ of the characteristic decomposition along the positive x axis in the focal plane ($z = 0$) for the tightly focused radially polarized GSM beam when the transverse coherence length δ_0 is (a) 10 mm, (b) 2 mm, (c) 1.3 mm, (d) 1.0 mm, (e) 0.5 mm, and (f) 0.05 mm. The solid vertical line indicates the point where the intensity has dropped to 10% of its maximum value.

necessarily highly polarized and therefore lacks 3D character [6], as shown in Fig. 2(a) with $1 \leqslant D \leqslant 2$. In this case essentially only the first term in the characteristic decomposition is present, as seen from Fig. 3(a) where $P_1 \approx 1$. Thus the polarization is close to a linearly polarized and circularly polarized state in the cases $D \approx 1$ and $D \approx 2$, respectively, and elliptically polarized in other cases. However, the orientation of the plane containing the ellipse may vary from point to point. Concerning the important region of high intensity, the field in the immediate neighborhood of the focal point is almost one dimensional (linearly polarized) with $D = 1.09$. This feature originates from a strong longitudinal field component which is generated around the focal point [11,12]. This region is surrounded by a ring of 2D (circularly polarized) light followed by a thicker ring of 1D light.

When the coherence width of the incident beam decreases, the polarimetric dimension starts to assume values larger than 2, hence expressing true three dimensionality of the field. In particular, an area with $D > 2$ is observed in the high-intensity region in all Figs. 2(b)–2(f). This behavior originates from the reduced intensity of the longitudinal component relative to the transverse components. Insight into this feature is gained from Figs. 3(b)–3(f), which demonstrate that the coefficients $P_2 - P_1$ and $1 - P_2$ in the characteristic decomposition dominate over P_1 close to the focal point. This holds the farther from the origin the lower δ_0 is, and eventually over the complete high-intensity region when $\delta_0 = 0.05$ mm. In Figs. 2(b)–2(d) the 3D unpolarized component $\hat{\mathbf{\Phi}}_u$ dominates near the origin, whereas in Figs. 2(e) and 2(f) the discriminating component $\hat{\mathbf{\Phi}}_m$ gives the strongest contribution to the polarization matrix. The largest possible focal-point value $D(0) = 2.96$ is found to be achieved when $\delta_0 = 1.3$ mm; the case shown in Fig. 2(c). As seen from Fig. 3(c) the polarization matrix is proportional to approximately $\hat{\mathbf{\Phi}}_u$ in this case. Thus, high-NA focusing of a radially polarized, partially spatially coherent GSM beam can generate a focal field which is essentially 3D unpolarized in a small region around the focus. For the

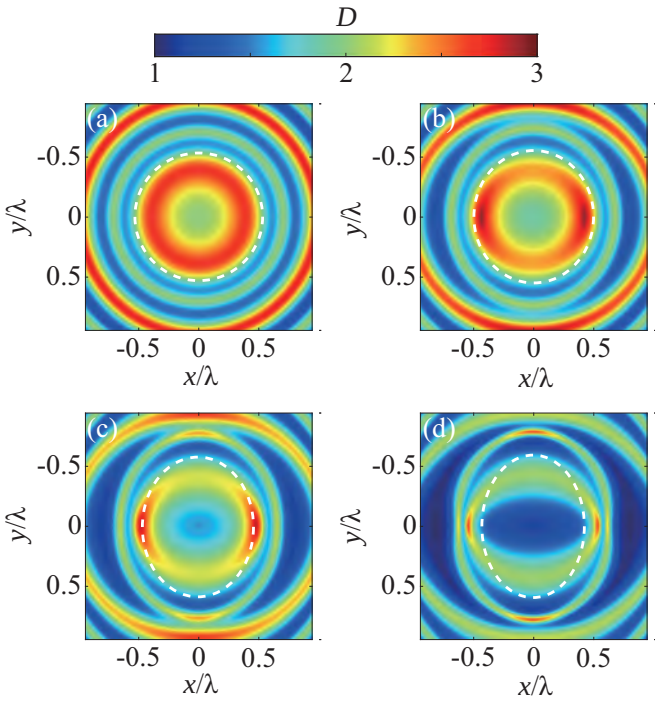

FIG. 4. Spatial distribution of the polarimetric dimension D in the focal plane ($z = 0$) of a tightly focused, partially polarized two-mode beam whose degree of polarization P_{2D} is (a) 0, (b) 0.3, (c) 0.6, and (d) 0.9. Inside the dashed circle the intensity is larger than 10% of its maximum value.

chosen wavelength we may estimate the radius of this region to be about 100 nm. In the limit $\delta_0 \to 0$ the distribution of the polarimetric dimension within the high-intensity region becomes nearly uniform with the value $D = 2.35$, indicating that the field is genuinely 3D in character over the whole focal domain. Figure 2 also demonstrates that the size of the focal intensity spot (illustrated by a dashed circle) increases with decreasing δ_0.

The degrees of nonregularity P_N of the total polarization matrix $\mathbf{\Phi}(\mathbf{r})$ and $P_N(\hat{\mathbf{\Phi}}_m)$ of the discriminating component are depicted in Fig. 3 with red and green solid curves, respectively. Within the important region where the intensity is larger than 10% of its maximum value (marked with a vertical line), the degree of nonregularity of the discriminating component can be high for the four largest coherence lengths [Figs. 3(a)–3(d)]. In Fig. 3(a) where $\delta_0 = 10$ mm, the component $\hat{\mathbf{\Phi}}_m$ is almost perfectly nonregular with $P_N(\hat{\mathbf{\Phi}}_m) \approx 1$ on a certain ring. However, in this case the weight factor $P_2 - P_1$ is virtually zero, so the contribution of $\hat{\mathbf{\Phi}}_m$ to the (practically fully polarized) total state $\mathbf{\Phi}(\mathbf{r})$ is negligible. But we observe the general trend that with reducing δ_0 the coefficient $P_2 - P_1$ increases while $P_N(\hat{\mathbf{\Phi}}_m)$ decreases. Therefore, we may expect a maximal degree of nonregularity of the whole state to take place for a certain δ_0, which is found to be $P_N \approx 0.2$ achieved close to $\delta_0 = 2$ mm plotted in Fig. 3(b). We further see that in all cases the field is essentially regular at the focal point, while with a decreasing coherence width the field becomes eventually regular throughout the high-intensity area as $P_N(\hat{\mathbf{\Phi}}_m)$, and hence P_N, approach zero.

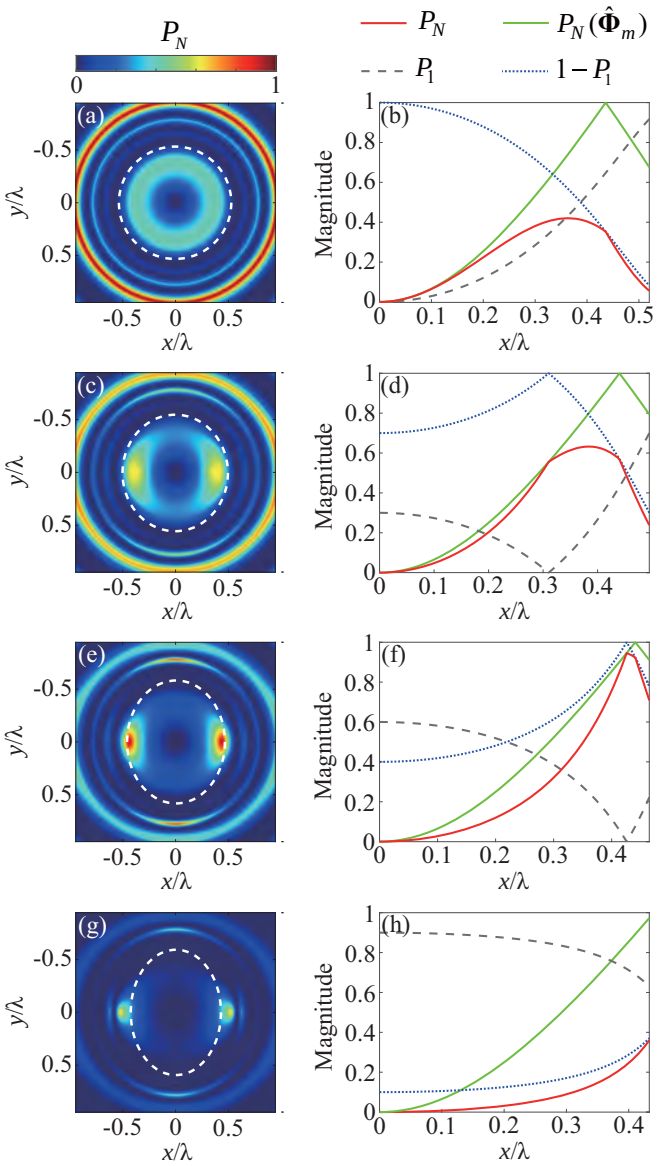

FIG. 5. Left: Spatial distribution of the degree of nonregularity P_N in the focal plane ($z = 0$) for a tightly focused, partially polarized two-mode beam. Right: Behavior of the associated degrees of nonregularity P_N and $P_N(\hat{\mathbf{\Phi}}_m)$ as well as the coefficients P_1 and $1 - P_1$ of the characteristic decomposition along the positive x axis in the focal plane. The degree of polarization P_{2D} of the incident beam is (a),(b) 0; (c),(d) 0.3; (e),(f) 0.6; and (g),(h) 0.9. Inside the dashed circle in the left panels the intensity is larger than 10% of its maximum value. The length scale in the right panels extends over the dashed circle regions of the left column.

B. Incoherent superposition of orthogonally polarized plane-wave modes

Figure 4 shows the polarimetric dimension D at the focal plane for a partially polarized incident beam whose CSDM is given in Eq. (18). The cases of Figs. 4(a)–4(d) correspond, respectively, to the degrees of polarization P_{2D} of 0, 0.3, 0.6, and 0.9 of the beam. The dotted curves isolate the region where the intensity is over 10% of its maximum value. The focal-plane distributions of the degree of nonregularity

P_N of the total polarization matrix $\mathbf{\Phi}(\mathbf{r})$ for the above P_{2D} values are plotted in Figs. 5(a), 5(c), 5(e), and 5(g), while Figs. 5(b), 5(d), 5(f), and 5(h) depict P_N (red solid line), $P_N(\hat{\mathbf{\Phi}}_m)$ (green solid line), P_1 (gray dashed line), and $1 - P_1$ (blue dotted line) along the positive x axis within the high-intensity region. For this beam type $P_2 = 1$ throughout the focal plane (not shown in Fig. 5) and hence the 3D unpolarized component $\hat{\mathbf{\Phi}}_u$ is not present in the characteristic decomposition.

We first observe that in the case of an unpolarized beam the region of high intensity is circular but becomes asymmetric when P_{2D} increases, i.e., the intensity ratio of the two orthogonal components grows. In other words, the state of partial polarization induces an asymmetric intensity spot at the focus, as found also in [37]. Similar behavior is seen in the contours of the polarimetric dimension, whose form transforms from circular to asymmetric with increasing P_{2D}. In the case of an unpolarized beam the field in the region around the origin is essentially two dimensional. This is surrounded by a thick ring of genuine 3D light, for which $D > 2$, and we see from Fig. 5(a) that this field is nonregular. The 3D character is solely due to the discriminating component $\hat{\mathbf{\Phi}}_m$ since $P_2 = 1$ in the characteristic decomposition. When P_{2D} increases the polarimetric dimension tends to decrease and for $P_{2D} = 0.9$ only a small region with $D > 2$ exists. For all P_{2D} values, when $D > 2$ within the area of strong intensity, the field is nonregular. Although not shown, in the limit $P_{2D} \to 1$ the polarimetric dimension obeys $1 \leqslant D \leqslant 2$ throughout the focal plane, as expected, since the focal light becomes fully polarized for which the electric field is necessarily restricted to a plane at every point [6]. Hence, due to the lack of 3D character, the field also becomes regular when $P_{2D} \to 1$, as indicated by Fig. 5(g).

Regarding the information provided by the right column of Fig. 5, we find from Fig. 5(b) that for an unpolarized incident beam the field around the focal point is to a good approximation 2D unpolarized since $P_1 = 0$ and the field is regular. With increasing distance from the origin the contribution of the nonregular discriminating component becomes stronger generating the ring of $D > 2$ in Fig. 4(a). At a certain distance in Fig. 5(b), the $\hat{\mathbf{\Phi}}_m$ state is perfectly nonregular with $P_N(\hat{\mathbf{\Phi}}_m) = 1$. This behavior is also visible in Figs. 5(d), 5(f) and 5(h). In Fig. 5(f) $P_1 = 0$ occurs near the point where the discriminating component is perfectly nonregular and hence the degree of nonregularity of the total field P_N can reach a value close to 1. In this case, the total field is in a perfect nonregular polarization state. In general, when P_{2D} increases, the contribution of $\hat{\mathbf{\Phi}}_p$ increases, whereas that of $\hat{\mathbf{\Phi}}_m$ decreases next to the focal point. Finally, we remark that for this beam type, notably larger degrees of nonregularity can be achieved in the focal region compared to the radially polarized GSM beam considered in Sec. IV A.

V. CONCLUSIONS

In this work, we examined two polarimetric descriptors, the polarimetric dimension and the degree of nonregularity, in the focal plane of a high-NA optical system. A radially (fully) polarized, spatially partially coherent GSM beam and a partially polarized beam composed of two mutually uncorrelated (spatially coherent) plane-wave modes were taken as the incident fields. The focal-field polarization matrix was computed within the Richards-Wolf formalism combined with a recently introduced fast calculation protocol. For both beams, rings where the polarimetric dimension exceeds the value of two, indicating a genuine 3D character of the field, were found in the focal region. For the two-mode beam also isolated spots of 3D light were observed. In these regions, the field, as a rule, is nonregular. In the limit of full spatial coherence and complete polarization the focal field becomes fully polarized. Consequently, as the electric field vector in such cases is restricted to a plane, which, however, may have different orientations at different points, the 3D features and nonregularity vanish. We also found that the GSM beam can produce a nanoscopic region around the focal point where the field is almost 3D unpolarized, and that the two-mode beam can generate a focus field which is virtually perfectly nonregular at certain locations. The results provide insight into the complicated and rich polarimetric structure of genuine 3D focal fields and may find use, for instance, in studies concerning focus-field design, particle manipulation, and focal spin.

ACKNOWLEDGMENTS

This research was supported by the National Natural Science Foundation of China (NSFC) (11525418, 91750201, 11874046, 11974218, and 11904247), the National Key Research and Development Project of China (2019YFA0705000), the Natural Science Foundation of the Jiangsu Higher Education Institutions of China (19KJB140017), the China Postdoctoral Science Foundation (2019M661915), the Natural Science Foundation of Shandong Province (ZR2019QA004), Innovation Group of Jinan (2018GXRC010), and the Academy of Finland (308393 and 310511). This work is a part of the Academy of Finland Flagship Program, Photonics Research and Innovation (PREIN) (320166). A.N. thanks the Jane and Aatos Erkko Foundation and J.J.G. thanks the Joensuu University Foundation. T.S. acknowledges the hospitality of the staff at Shandong Normal University during his visit.

[1] C. Brosseau, *Fundamentals of polarized light: A statistical optics approach* (Wiley, New York, 1998).

[2] J. J. Gil and R. Ossikovski, *Polarized light and the Mueller matrix approach* (CRC Press, New York, 2016).

[3] L. Novotny and B. Hecht, *Principles of nano-optics*, 2nd ed. (Cambridge University Press, Cambridge, 2012).

[4] J. J. Gil, A. T. Friberg, T. Setälä, and I. San José, Structure of polarimetric purity of three-dimensional polarization states, Phys. Rev. A **95**, 053856 (2017).

[5] J. J. Gil, Polarimetric characterization of light and media, Eur. Phys. J. Appl. Phys. **40**, 1 (2007).

[6] A. Norrman, A. T. Friberg, J. J. Gil, and T. Setälä, Dimensionality of random light fields, J. Eur. Opt. Soc.- Rapid Publ. **13**, 36 (2017).
[7] J. J. Gil, A. Norrman, A. T. Friberg, and T. Setälä, Intensity and spin anisotropy of three-dimensional polarization states, Opt. Lett. **44**, 3578 (2019).
[8] J. J. Gil, A. Norrman, A. T. Friberg, and T. Setälä, Polarimetric purity and the concept of degree of polarization, Phys. Rev. A **97**, 023838 (2018).
[9] J. J. Gil, A. Norrman, A. T. Friberg, and T. Setälä, Nonregularity of three-dimensional polarization states, Opt. Lett. **43**, 4611 (2018).
[10] A. Norrman, J. J. Gil, A. T. Friberg, and T. Setälä, Polarimetric nonregularity of evanescent waves, Opt. Lett. **44**, 215 (2019).
[11] K. S. Youngworth and T. G. Brown, Focusing of high numerical aperture cylindrical-vector beams, Opt. Express **7**, 77 (2000).
[12] R. Dorn, S. Quabis, and G. Leuchs, Sharper Focus for a Radially Polarized Light Beam, Phys. Rev. Lett. **91**, 233901 (2003).
[13] T. Bauer, P. Banzer, E. Karimi, S. Orlov, A. Rubano, L. Marrucci, E. Santamato, R. W. Royd, and G. Leuchs, Observation of optical polarization Möbius strips, Science **347**, 964 (2015).
[14] Y. Zhao, J. S. Edgar, G. D. M. Jeffries, D. McGloin, and D. T. Chiu, Spin-to-Orbital Angular Momentum Conversion in a Strongly Focused Optical Beam, Phys. Rev. Lett. **99**, 073901 (2007).
[15] M. Neugebauer, T. Bauer, A. Aiello, and P. Banzer, Measuring the Transverse Spin Density of Light, Phys. Rev. Lett. **114**, 063901 (2015).
[16] G. Rui, Y. Li, S. Zhou, Y. Wang, B. Gu, Y. Cui, and Q. Zhan, Optically induced rotation of Rayleigh particles by arbitrary photonic spin, Photon. Res. **7**, 69 (2019).
[17] S. Roy, K. Ushakova, Q. van den Berg, S. F. Pereira, and H. P. Urbach, Radially Polarized Light for Detection and Nanolocalization of Dielectric Particles on a Planar Substrate, Phys. Rev. Lett. **114**, 103903 (2015).
[18] B. Richards and E. Wolf, Electromagnetic diffraction in optical systems II. Structure of the image field in an aplanatic system, Proc. R. Soc. London, Ser. A **253**, 358 (1959).
[19] J. J. Stamnes, *Waves in Focal Regions* (Hilger, Bristol, 1986).
[20] M. R. Foreman and P. Török, Focusing of spatially inhomogeneous partially coherent, partially polarized electromagnetic fields, J. Opt. Soc. Am. A **26**, 2470 (2009).
[21] R. Tong, Z. Dong, Y. Chen, F. Wang, Y. Cai, and T. Setälä, Fast calculation of tightly focused random electromagnetic beams: Controlling the focal field by spatial coherence, Opt. Express **28**, 9713 (2020).
[22] J. J. Gil, J. M. Correas, P. A. Melero, and C. Ferreira, Generalized polarization algebra, Monogr. Semin. Mat. Garcia Galdeamo **31**, 161 (2004).
[23] L. Mandel and E. Wolf, *Optical coherence and quantum optics* (Cambridge University Press, Cambridge, 1995).
[24] J. Tervo, T. Setälä, and A. T. Friberg, Theory of partially coherent fields in the space-frequency domain, J. Opt. Soc. Am. A **21**, 2205 (2004).
[25] R. Martínez-Herrero, P. M. Mejías, and F. Gori, Genuine cross-spectral densities and pseudo-modal expansions, Opt. Lett. **34**, 1399 (2009).
[26] S. Yang, S. A. Ponomarenko, and Z. Chen, Coherent pseudo-mode decomposition of a new partially coherent source class, Opt. Lett. **40**, 3081 (2015).
[27] X. Chen, J. Li, S. M. H. Rafsanjani, and O. Korotkova, Synthesis of I_m-Bessel correlated beams via coherent modes, Opt. Lett. **43**, 3590 (2018).
[28] H. Mao, Y. Chen, S. A. Ponomarenko, and A. T. Friberg, Coherent pseudo-mode representation of partially coherent surface plasmon polaritons, Opt. Lett. **43**, 1395 (2018).
[29] J. C. G. de Sande, R. Martínez-Herrero, G. Piquero, M. Santarsiero, and F. Gori, Pseudo-Schell model sources, Opt. Express **27**, 3963 (2019).
[30] Y. Chen, A. Norrman, S. A. Ponomarenko, and A. T. Friberg, Partially coherent surface plasmon polariton vortex fields, Phys. Rev. A **100**, 053833 (2019).
[31] Y. Dong, Y. Cai, C. Zhao, and M. Yao, Statistics properties of a cylindrical vector partially coherent beam, Opt. Express **19**, 5979 (2011).
[32] F. Wang, Y. Cai, Y. Dong, and O. Korotkova, Experimental generation of a radially polarized beam with controllable spatial coherence, Appl. Phys. Lett. **100**, 051108 (2012).
[33] J. Tervo, T. Setälä, and A. T. Friberg, Degree of coherence for electromagnetic fields, Opt. Express **11**, 1137 (2003).
[34] D. Voelz, X. Xiao, and O. Korotkova, Numerical modeling of Schell-model beams with arbitrary far-field patterns, Opt. Lett. **40**, 352 (2015).
[35] M. W. Hyde IV, Stochastic complex transmittance screens for synthesizing general partially coherent sources, J. Opt. Soc. Am. A **37**, 257 (2020).
[36] M. Leutenegger, R. Rao, A. Leitgeb, and T. Lasser, Fast focus field calculations, Opt. Express **14**, 11277 (2006).
[37] K. Lindfors, T. Setälä, M. Kaivola, and A. T. Friberg, Degree of polarization in tightly focused optical fields, J. Opt. Soc. Am. A **22**, 561 (2005).